



## CuO NPs incorporated single and double junction polymer solar cells

Aruna P. Wanninayake<sup>1</sup>, Benjamin C. Church<sup>1</sup>, Nidal Abu-Zahra<sup>1</sup>

<sup>1</sup> *Materials Science and Engineering, University of Wisconsin-Milwaukee, 3200 North Cramer Street, Milwaukee, WI 53201, USA.*

Received 25 Apr 2016; Revised 19 Aug 2016; Accepted 25 Aug 2016

### Abstract

Multi-junction architecture is an attractive method to overcome the efficiency limit of single-junction photovoltaic solar cells. Series-connected multi-junction polymer solar cells (PSCs) have attracted much attention during the past decade. In this study, single and double layer polymer solar cells were fabricated incorporating copper oxide and zinc oxide nanoparticles (CuO and ZnO NPs) in the active layers. Thermal annealing treatment was applied to the single and double junction devices at 200°C to optimize the nanoscale morphology. The single layer device produced 2.963% power conversion efficiency and it was reduced to 1.102% in the double junction solar cell. However, the enhanced morphological and optoelectronic properties attained by applying thermal annealing slightly increased the power conversion efficiency. Meanwhile, the external quantum efficiency (EQE) increased from 32.4% to 37%, showing an enhancement of 12.4% with the thermal annealing treatment.

**Keywords:** ZnO nanoparticles, CuO nanoparticles, EQE, UV-visible spectroscopy, PSCs

### 1. Introduction

Photovoltaic (PV) polymer solar cells (PSCs), which are based on solution-processed conjugated polymer donor and fullerene derivative acceptor materials, have attracted much attention in recent years due to their advantages of easy fabrication, simple device structure, low cost, light weight, and capability to be fabricated into flexible devices [1-5]. At the present time, 10% power conversion efficiency (PCE) is reached [6, 7] for a single-junction solar cell. To compete with the conventional inorganic cells, the power conversion efficiencies of the organic devices should be increased. Compared to inorganic solar cells, polymer solar cells (PSCs) usually have insufficient light absorption due to the thin active layer, which is restricted by the short exciton diffusion length and low carrier mobility [8, 9]. These factors limit the maximum thickness of the active layer of light absorption. Efficient conversion of solar energy requires the compounds to absorb strongly in the visible region of the spectrum.

To increase the absorption band within the solar spectrum, multi-junction solar cells are employed and thus increase the power conversion efficiency. The multi-junction solar

\* ) For Correspondence. Tel: + (01) (414) 229-2668, Fax: + (01) 4142296958, E-mail: nidal@uwm.edu

cells are capable of reducing the sub-bandgap transmission loss of photons, which is the major loss mechanism in solar cells [10, 11]. Many researchers worked on enhancing the PCE of polymer based solar cells by fabricating multi junction solar cells and the PCE has reached more than 10% in organic tandem cells. This efficiency is approximately close to the efficiency of a single-junction organic cell, indicating that progress in the field of multi-junction organic solar cells is still possible. To improve the optical absorption of the solar energy by organic solar cells, materials with a wide absorption band should be designed, or different narrow-band absorbers have to be incorporated in multiple junctions [12, 13]. When two (or more) donor materials with non-overlapping absorption spectra are utilized in a multi-junction solar cell, a broader range of the solar spectrum can be achieved. Many approaches for organic multiple junction solar cells have been reported in the past years, depending on the materials used for the active layer and the proper separation or recombination layer. Hadipour *et al* [14] reported 0.57% power conversion efficiency for polymer tandem solar cell consisting of two subcells with two different materials. Kim *et al* [15] demonstrated a 6.5% PCE for double junction tandem structure. Also, nanoparticles of metals and transition metals oxides are an important class of semiconductors having applications in multiple technical fields like solar energy transformation [16, 17]. In our previously reported work, copper oxide nanoparticles (CuO NPs) were successfully incorporated into the P3HT/ PC70BM active layer. The PCE was increased in single layer PSCs due to enhanced carrier generation ability of P3HT/PCBM/CuO NPs thin films [18, 19]. Therefore, CuO NPs could be used to increase the PCE in double junction solar cell devices as well.

In this study, we are demonstrating a low bandgap organic material design for double junction PSCs. The performance parameters of the best single and double layer solar cell devices are compared and presented in this paper. Also, we will discuss the synthesis process, and the requirements for characterization of single- and multi- junction polymer solar cells.

## **2. Experimental methods**

### **2.1 Materials**

Active layer materials, P3HT and PC70BM were purchased from Rieke Metals and SES Research; respectively. Nanoparticles of ZnO (18 nm diameter) and CuO (35-50nm diameter) were purchased from nanocs.com. PEDOT/PSS mixed in distilled water was obtained from Sigma Aldrich and it was mixed with an equal amount of distilled water. Glass substrates measuring 24 x 80 x 1.2 mm ( $12 \Omega/\text{cm}^2$ ) with an ITO conductive layer of 25-100 nm were purchased from nanocs.com. Aluminium coils with a diameter of 0.15 mm were purchased from Ted-Pella, Inc. (tedpella.com). All processing and characterization work of the PSC devices were conducted under the same experimental conditions.

### **2.2 Solar Cells Fabrication**

The double junction cells were processed according to the following method. The conductive glass substrates were ultrasonically cleaned with ammonium hydroxide, hydrogen peroxide, distilled water, methyl alcohol, and isopropyl alcohol; successively. The fabrication of double junction solar cells was done in an  $\text{N}_2$  filled glove box. The ZnO nanoparticles were dispersed in pure ethanol to make a solution with a concentration of  $20 \text{ mg ml}^{-1}$ . The P3HT-PC70BM blend was obtained by diluting same amounts of regioregular P3HT and PC70BM (10 mg each) with 2ml of chlorobenzene ( $\text{C}_6\text{H}_5\text{Cl}$ ) and mixing for 14

hours at 60°C. CuO NPs were dispersed in 2ml of C<sub>6</sub>H<sub>5</sub>Cl and were added to the mixture, so that the weight ratios of P3HT/PCBM/CuO-NPs in the final blend was 10:10:0.6 mg.

The solar cell devices were spun coated in a glove box filled with N<sub>2</sub> atmosphere. A 40 nm-thick PEDOT/PSS layer, which serves as a thin hole-transport layer, was spun coated at a rotational velocity of 4000 rpm, followed by heating at 120°C for 20 minutes in air. When the temperature of the samples reached the ambient temperature, the blends with P3HT:PC70BM: CuO NPs active layer and ZnO solution were spun coated for two minutes at 1000 rpm and 2000 rpm; respectively. The second PEDOT:PSS layer was applied on the ZnO NPs layer and annealed at 120 °C for 10 min. Then the second subcell active layer of P3HT/PC70BM (1:1) solution was then spin-casted at 1000 rpm on top of the ZnO layer, the thickness of this layer is about 100–120 nm.

Single junction solar cells were fabricated using the same materials and method. After fabricating the PEDOT/PSS layer with a thickness of 40 nm on the ITO substrate, the sample is baked at 120 °C for 15 minutes. This serves as a thin hole-transport layer. Once the sample cooled to room temperature, a hybrid solution containing P3HT/PC70BM/CuO NPs was deposited by spin-coating at 1000 rpm for one minute, which leads to a film thickness of about 100-150 nm. The purpose of this layer is to serve as the active layer. Thermal annealing was performed on both single and double junction devices, after Al electrode deposition, inside an inert oven at 200°C for 30 minutes. The structures of the fabricated solar cell devices are schematically presented in Fig. 1.

### 2.3 Solar Cells Characterization

The current density–voltage (J-V) characterization was carried out for all double junction PSCs using a UV solar simulator with an AM 1.5G filter and a lamp intensity of 100 mW/cm<sup>2</sup>. A source meter (Keithley 2400) was used to obtain the J-V measurements. Device parameters such as short circuit current ( $J_{sc}$ ), open circuit voltage ( $V_{oc}$ ), fill factor (FF) and power conversion efficiency (PCE) were recorded under ambient conditions. A quantum efficiency measurement kit (Newport-425) embedded in the solar cell simulator was used to obtain EQE values. A PerkinElmer LAMBDA 650 spectrophotometer was used to obtain the optical properties of cells containing varying amounts of ZnO NPs. Agilent 5420 atomic force microscope (AFM) was used to analyze the surface morphology of the devices. Pico Image Basics and Gwyddion software were used to determine the root mean square surface roughness ( $\sigma_{rms}$ ).

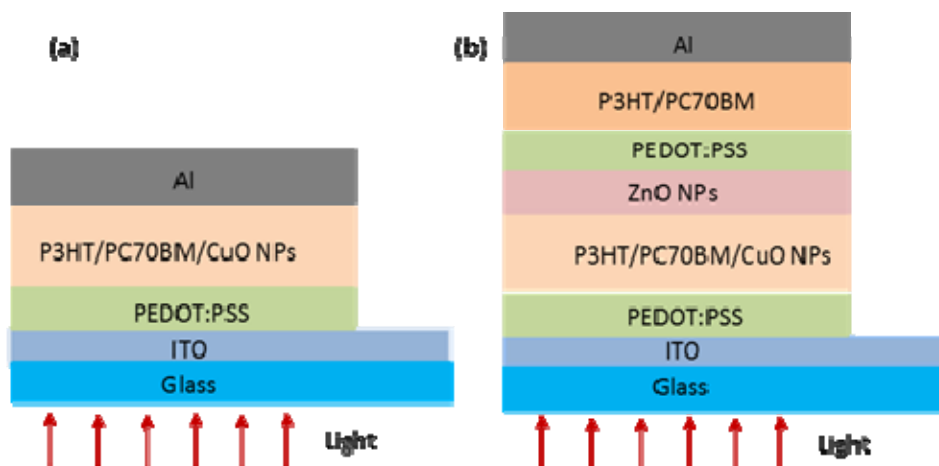


Fig. 1: Schematic representation of: (a) single layer PSC (b) double layer PSC

### 3. Results and Discussion

In a double-junction tandem cell, the high energy photons of the incident light are harvested in the front subcell i.e., back subcell operates under suppressed light conditions. Therefore, higher photocurrent density is needed for this subcell to avoid the current-limiting [20, 21]. The photovoltaic parameters; such as short-circuit current density ( $J_{sc}$ ), open-circuit voltage ( $V_{oc}$ ), fill factor and power conversion efficiency; which is defined as the ratio of the products of  $V_{oc}$ ,  $J_{sc}$  and FF to the total incident power density is shown in Table 1.

A series of unheat-treated and heat-treated TeO<sub>2</sub> - Na<sub>2</sub>O – MgO glass system doped with Eu<sup>3+</sup> have successfully been prepared by melt-quenching technique.

Table 1: Device parameters of single and double layer solar cells

Sample	$J_{sc}$ (A/cm <sup>2</sup> )	$V_{oc}$ (V)	FF(%)	$R_s$ (Ω/cm <sup>2</sup> )	PCE(%)
Single layer device	6.484	0.673	68.00	16	2.963
Single layer device (after annealing)	9.149	0.610	67.31	12	3.701
Double layer device	2.702	0.658	63.35	53	1.102
Double layer device (after annealing)	3.470	0.660	64.76	45	1.463

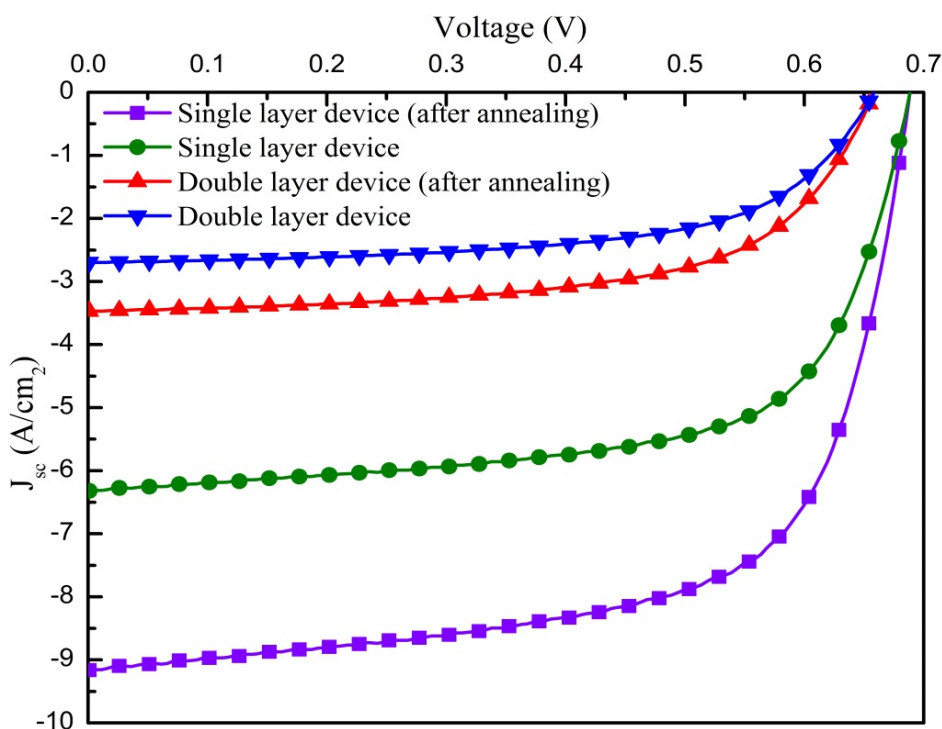


Fig. 2:  $J$ - $V$  characteristics of single and double layer polymer solar cells

Fig. 2 shows the photocurrent density–voltage (J-V) curves measured under standard AM1.5 solar illumination. The best single junction solar cell exhibited the highest PCE of 2.963%. The device provides a high short-circuit current density ( $J_{sc}$ ) of  $6.484 \text{ mA cm}^{-2}$  and a concomitantly high EQE. In addition, the fill factor ( $FF = 0.68$ ) is also high, indicating efficient charge carrier collection, even at low electric fields over the absorber layer. After thermal annealing,  $J_{sc}$  increased to  $9.149 \text{ mA/cm}^2$ , and FF remained almost the same. As a result, PCE increased to 3.701%, leading to a 24% enhancement in the cells containing 0.6 mg of CuO NPs.

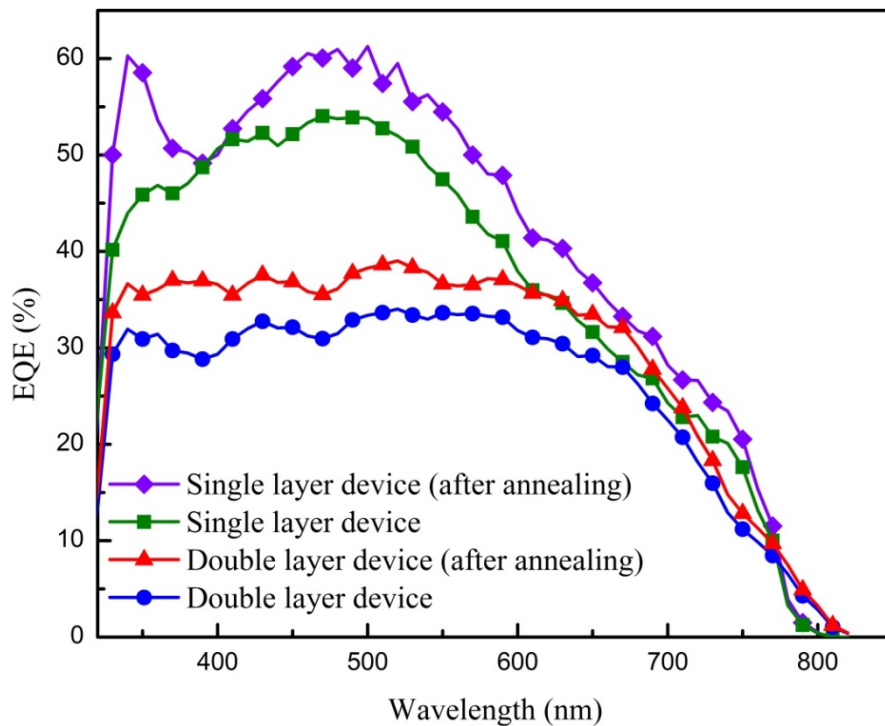


Fig. 3: EQE of the single and double solar cells

However, in the J-V characteristic of the optimum double-junction device, the short circuit current density was decreased to  $2.702 \text{ mA/cm}^2$ , which accounts for a 58% decrement. The lower current density decreased the power conversion efficiency (PCE) to 1.102%; in addition, the fill factor decreased from 68.00% to 63.35% with 6.8% decrement. The performance parameters of the double-junction device after annealing revealed an improvement in  $J_{sc}$  to  $3.47 \text{ mA/cm}^2$  with a 22% increment. This enhanced short circuit current density proportionally improved PCE from 1.102% to 1.463%. Following a similar trend, the fill factor increased from 63.35 to 64.76% after the annealing treatment. The thermal annealing treatment contributed for about 24% increase in PCE as a result of slightly improved  $J_{sc}$  and FF. The open circuit voltage ( $V_{oc}$ ) is controlled by the energetic relationship between the donor and the acceptor. The energy difference between the highest occupied molecular orbit (HOMO) of the donor and the lowest unoccupied molecular orbit (LUMO) of the acceptor is known to most closely and linearly correlate with the  $V_{oc}$  [22, 23]. However,  $V_{oc}$  did not change significantly in both the single and double layer devices.

External quantum efficiency (EQE) measurements were performed to investigate the spectral response of the optimum double layer device as well as the best single layer solar cell. The EQE or the incident photon to current conversion efficiencies (IPCE) measurements describe the ratio between the incident photons on the solar cell from the input source, and the generated free charge carriers by the solar cell. As shown in Fig. 3, the

peak intensity of the EQE curve of the double layer cell is decreased compared to the single layer solar cell. The corresponding EQE measurements (peak values) were observed at 54% and 32.4% for the double layer and single layer solar cells; respectively. However, after annealing the peak values of the EQE for the double layer and single layer solar cell increased to 37% and 61% in the wavelength range from 350nm to 700nm respectively.

The major factors responsible for a lower EQE and PCE could be attributed to the increased series resistance ( $R_S$ ) and reduced optical absorption. The series resistance ( $R_S$ ) increased from  $16 \Omega \text{ cm}^2$  (single layer device) to  $53 \Omega \text{ cm}^2$  (double layer device), as shown in Table 1. It is well known that the  $R_S$  directly influences the fill factor (FF) [24, 25]. Therefore, it can be concluded that the reduced FF could be due to the increased  $R_S$ . The optical absorption of the double layer device followed a similar trend. The UV-Vis spectra are shown in Fig. 4.

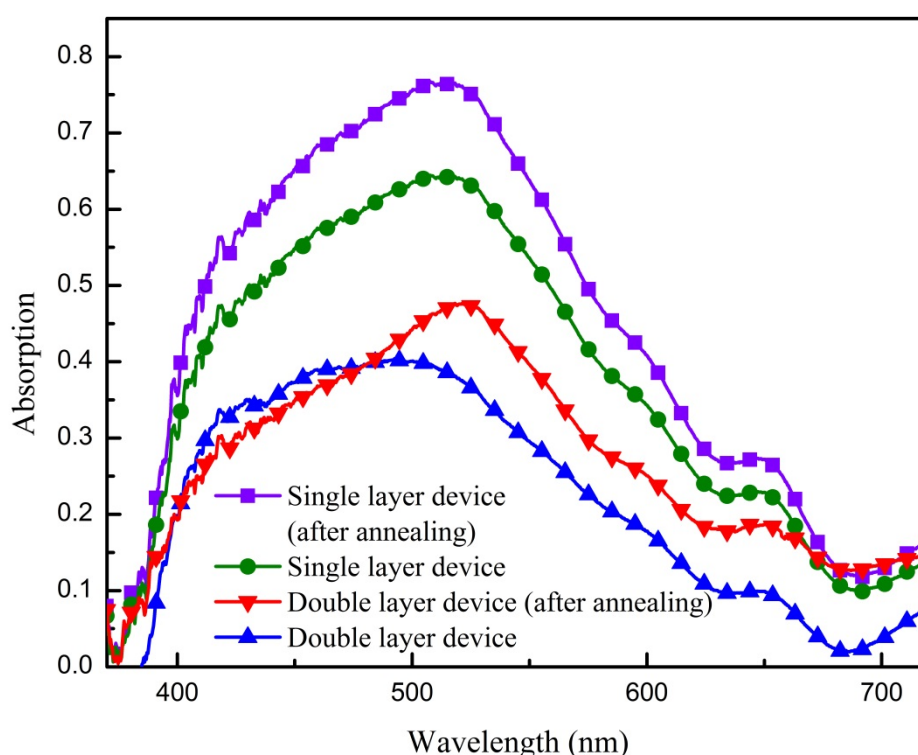


Fig.4: Optical absorption spectra of single and double solar cells

In order to minimize the thermalization losses, multi-junction polymer solar cells use a large bandgap material as the front absorber. The front cells generally harvest high-energy photons. In addition, small bandgap absorbers are used for the back layer to absorb low-energy photons. CuO NPs remarkably enhance the optical absorption properties of P3HT/PC70BM thin films in the solar cell devices [26, 27]. However, the lower photo absorption could be due to the increased thermalization losses at the front cell. Franeker *et al.* [28] state that the poor device performance of P3HT:PCBM cells can be observed when ZnO was coated on top of P3HT:PCBM due to the crystallization of P3HT, which changes the morphology of the upper ZnO film and other top layers.

The results from EQE concur with the results obtained from UV-Vis. It is clear that the absorption of P3HT:PC70BM/CuO NPs cell in the range of 420 nm to 600 nm is enhanced after thermal annealing. The improvement of EQE can be attributed to the

increased hole and electron polaron motilities, charge collection at the electrodes, and photon absorption. The photon absorption coefficient describes the photon absorption capacity of the thin films. The optical absorption coefficient, band gap, and the thickness of the photoactive layer are the major determinants of photon absorption yield. Furthermore, in the double layer solar cell, optical absorption was enhanced by incorporating CuO NPs in the front cell of the device. Assembling a ZnO electron transport layer inside the device provides extremely high electron transporting facility to the electrodes. Compared to the electron mobility in  $\text{TiO}_x$  thin films ( $1.7 \times 10^{-4} \text{ cm}^2 \text{ V}^{-1} \text{ s}^{-1}$ ) [29], the ZnO NPs layers have higher electron mobility ( $6.6 \times 10^{-2} \text{ cm}^2 \text{ V}^{-1} \text{ s}^{-1}$ ) [30]. Hence, ZnO structure gives high momentum to the moving electrons towards the cathode, thus enhancing the exciton dissociation rate. Thermal annealing introduces higher crystallinity and smaller crystallite size in the thin film, thus leading to better electron mobility. The annealing treatment of P3HT near the glass transition rearranges the molecular ordering of the internal microstructure [31, 32]. This leads to an increase in the extent of carrier diffusion of P3HT polymer across the PCBM phase, thus improving  $J_{sc}$  in the photovoltaic performance.

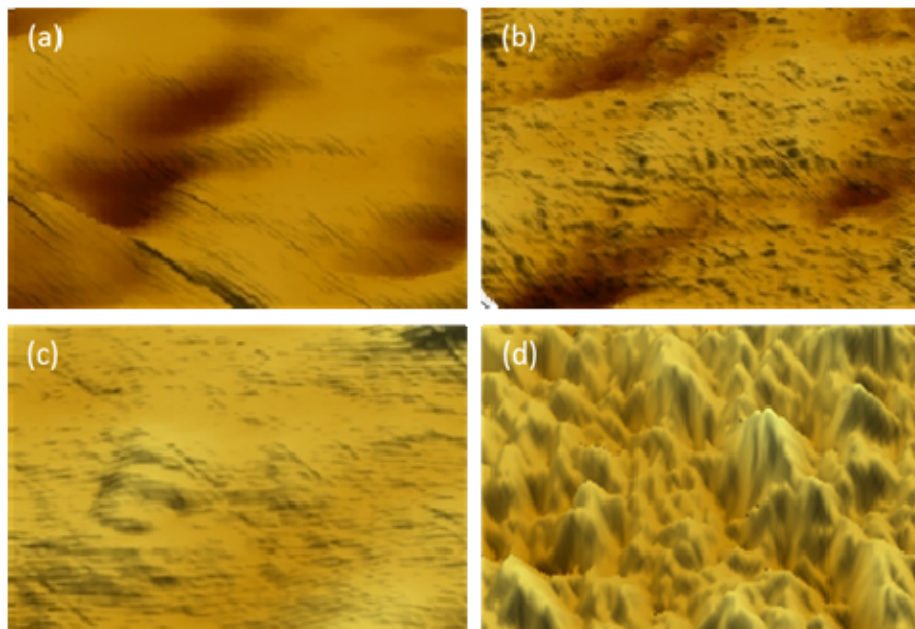


Fig. 5: AFM images of active layers with (a) P3HT:PC70BM film before annealing, (b) P3HT:PC70BM/CuO NPs film before annealing, (c) P3HT:PC70BM film after annealing, (d) P3HT:PC70BM/CuO NPs film after annealing

The AFM surface images of the active layer of both sub cells (P3HT:PC70BM/CuO NPs and P3HT:PC70BM), before and after thermal annealing, are shown in Fig. 5. The AFM roughness values of the P3HT/PC70BM/CuO NPs films and P3HT/PC70BM layer have increased after thermal annealing. The measured root-mean-square roughness ( $\sigma_{rms}$ ) value of the P3HT/PC70BM/CuO NPs layer was 0.32nm, and it increased to 0.84nm after the annealing treatment. The  $\sigma_{rms}$  value of the P3HT/PC70BM layer was 0.12nm and it increased to 34nm after the annealing treatment. An increase in surface roughness allows more space for P3HT crystallites to form; thereby increasing crystallinity. This can be attributed to increased nano-scale phase separation between the crystalline P3HT and the PC70BM acceptor with thermal annealing [33]. Furthermore; these roughened surfaces provide better interfacial contact between the layers and hence enhance the charge mobility between the thin films.

#### 4. Conclusion

In this study, CuO NPs incorporated single and double layer solar cells were fabricated. The power conversion efficiency (PCE) of the single and double-junction polymer–fullerene solar cells ranged between 2.963% and 1.102%, respectively. However, after thermal annealing of the double junction device, the PCE increased from 1.102% to 1.463% due to enhanced P3HT crystallinity and increased nano-scale phase separation between the crystalline P3HT and the PC70BM acceptor domains. The EQE spectra followed a similar trend; the peak value of EQE decreased in the double junction device and it increased after thermal annealing. The series resistance ( $R_s$ ) remarkably increased in the double junction device and the optical absorption decreased in comparison with the single junction device. However, after annealing treatment, the series resistance decreased and the optical absorption slightly increased. AFM analysis shows an increase in the surface roughness of the active layers of single and double junction devices after thermal annealing, which resulted in a larger interface area between the mutual layers.

#### References

- [1] N. Abu-Zahra and M. Algazzar. *J. Sol. Energy Eng.* **136** (2) (2013) 021023
- [2] M. Manceau, D. Angmo, M. Jorgensen, and F.C. Krebs, *Org. Electron.* **12** (2011) 566-574
- [3] C. H. Michael and D. Ali. *Applied Phys. Rev.* **2** (2014) 014008
- [4] A.P. Wanninayake, B.C. Church, N. Abu-Zahra. *J. Sustainable Energy Eng.* **3** (4) (2016) 333-342(10)
- [5] A.P. Wanninayake, S. Li, B.C. Church, N. Abu-Zahra. *International Journal of Renewable Energy Research*, **5**(4) (2015) 1080-1091
- [6] J.-D Chen, C.Cui, Y.Q. Li, L. Zhou, Q.-D. Ou, C. Li, Y. Li, J.-X. Tang. *Adv. Mater.* **27** (2015) 1035–1041
- [7] Y. Liu, J. Zhao, Z. Li, C. Mu, W. Ma, H. Hu, K. Jiang, H. Lin, H. Ade, H. Yan. *Nat. Commun.* **5** (2014) 5293–5300
- [8] D. J. D. Moet, P. de Bruyn, P.W.M. Blom. *Appl. Phys. Lett.* **96** (2010) 153504-153506
- [9] W. Li, A. Furlan, K.H. Hendriks, M.M. Wienk, R.A.J. Janssen, *J. Am. Chem. Soc.* **135** (2013) 5529–5532
- [10] A. R. b. M. Yusoff, W. J. da Silva, H. P. Kim, J. Jang. *Nanoscale* **5** (2013) 11051–11057
- [11] M.-R Choi, T.-H. Han, K.-G. Lim, S.-H. Woo, D. H. Huh, T.-W. Lee, *Angew. Chem.* **123** (2011) 6398–6401
- [12] T. Kuwabara, Y. Kawahara, T. Yamaguchi, K. Takahashi. *ACS Appl. Mater. Interfaces* **1** (2009) 2107–2110
- [13] Y. Xu, Z. Sui, B. Xu, H. Duan, X. Zhang, *J. Mater. Chem.* **22** (2012) 8579–8584
- [14] A. Hadipour, B. de Boer, P. W. M. Blom, *Adv. Funct. Mater.* **18** (2008) 169–181
- [15] J. Y. Kim, K. Lee, N. E. Coates, D. Moses, T.-Q. Nguyen, M. Dante, A. J. Heeger, *Science* **317** (2007) 222
- [16] R. P. P. Singh, I.S. Hudiara, S. Panday, P. Kumar, S. B. Rana. *Int. J. Nanoelectronics and Materials*, **9** (2016) 1-8
- [17] A.M. Shehap, D. S.Akil, *Int. J. Nanoelectronics and Materials*, **9** (2016) 17-36
- [18] A.P. Wanninayake, S. Gunashekar, S. Li, B.C. Church, N. Abu-Zahra *J. Sol. Energy Eng.* **137** (2015) 031016

- [19] A.P. Wanninayake, S. Li, B.C. Church, N. Abu-Zahra. *AIMS Materials Science*, **3** (1) (2015) 35-50
- [20] J. Lee, H. Kang, J. Kong, K. A. Lee. *Adv. Energy Mater.* **4** (2014) 1301226
- [21] Y. Zhou, C. Fuentes-Hernandez, J.W. Shim, T.M. Khan, B. Kippelen. *Energy Environ. Sci.* **5** (2012) 9827–9832
- [22] B.P. Nguyen, T. Kim, C.R. Park, J. Nanomater. 2014 (2014) 243041
- [23] B. Eisenhawer, S. Sensfuss, V. Sivakov, M. Pietsch, G. Andra F. Falk *Nanotechnology*, **22** (2011) 315401
- [24] A.P. Wanninayake, B.C. Church, N. Abu-Zahra. *AIMS Materials Science*, **3**(3) (2016) 927-937
- [25] A.P. Wanninayake, S. Gunashekar, S. Li, B.C. Church, N. Abu-Zahra *J. Sustainable Energy Eng.* **3**(2) (2015) 107-126(20)
- [26] F.-C.Chen, S.-C Chien *J. Mater. Chem.* **19** (2009) 6865–6869
- [27] H. Kang, J. Lee, S. Jung, K. Yu, S. Kwon, S. Hong, S. Kee, S. Lee, D. Kim, K. Lee. *Nanoscale*, **5** (2013) 11587– 1591
- [28] J.J. van Franeker, W. Voorthuijzen, H. Gorter, K.H. Hendriks, R.A. Janssen, A. Hadipour, R. Andriessen, Y. Galagan. *Sol. Ener. Mater. Sol. Cells*, **117** (2013) 267–272
- [29] J. Y. Kim, S. H. Kim, H. H. Lee, K. Lee, W. Ma, X. Gong and A. J. Heeger. *Adv. Mater*, **18** (2006) 572
- [30] L. Roest, J. J. Kelly, D. Vanmaekelbergh and E. A. Meulenkaamp. *Phys. Rev. Lett.* **89** (2002) 036801
- [31] V. Djara and J. Bernède. *Thin Solid Films*, **493** (2005) 273
- [32] T. Oo, N. Mathews, T. Tam, G. Xing, T. Sum, A. Sellinger, L. Wong, S. Mhaisalkar. *Thin Solid Films*, **518** (2010) 5292
- [33] A. Wanninayake, S. Gunashekar, S. Li, B. C. Church and N. Abu-Zahra. *Semicond. Sci. Technol.* **30** (2015) 064004

